

Ion distribution around a charged rod in one and two component solvents: Preferential solvation and first order ionization phase transition

Ryuichi Okamoto* and Akira Onuki†

Department of Physics, Kyoto University, Kyoto 606-8502, Japan

(Dated: March 13, 2019)

In one and two component solvents, we calculate the counterion distribution around a charged rod treating the degree of ionization α as an annealed variable dependent on its local environment. In the one component case, α is determined under various conditions without and with salt. In the two component case, we take into account the preferential solvation of the counterions and the ionized monomers and the short-range interaction between the rod and the solvent without salt. It then follows a composition-dependent mass action law. Mesoscopic variations of the composition and the counterions are produced around a charged rod, which sensitively depend on various parameters of the molecular interactions. Furthermore, we predict a first order phase transition of weak-to-strong dissociation for strong preferential solvation. It can occur in expanded states of a polymer chain. This transition line starts from a point on the solvent coexistence curve and ends at a critical point in the plane of the temperature and the solvent composition. The composition change around a charged rod is long-ranged near the solvent critical point.

I. INTRODUCTION

Polyelectrolyte systems are known to be extremely complicated^{1,2,3,4,5,6,7,8,9,10}. Examples include biologically important polyelectrolytes, like DNA, actin filaments or microtubules, and synthetic polyelectrolytes. In such charged polymer systems, the Coulomb repulsion among ionized monomers can induce a number of conformation changes of a chain. The Coulomb attraction among counterions and an ionized chain can result in condensation of counterions at large counterion contents (the Manning-Oosawa counterion condensation). In practice, it is important that the phase behavior of polyelectrolytes strongly depends on the degree of ionization. For example, hydrophobic polymer chains become soluble in water-like solvents with slight ionization. In this paper, we further investigate two complex aspects of polyelectrolytes, which have not yet been fully discussed.

First, the ionization (or dissociation) process on the chains should be treated as a chemical reaction in many polyelectrolytes containing weak acidic monomers^{6,11,12,13,14,15}. The degree of ionization α is an annealed fluctuating variable governed by the mass action law and dependent on the local values of the counterion density and the composition (in mixture solvents). All these quantities are self-consistently coupled with the electric potential obeying the Poisson equation. Inhomogeneity of α is particularly crucial in structure formations and phase separation¹⁵. However, even when α is homogeneous, α is a complex quantity sensitively dependent on various conditions. It can be small in solvents with low dielectric constant and can increase considerably in highly polar solvents.

Second, complex effects are known to be induced in polyelectrolytes when a second fluid component (co-solvent) is added to a water-like solvent. For example, precipitation of DNA has been widely observed with addition of (less polar) alcohol such as ethanol to water^{16,17,18,19}. Here the alcohol added is excluded from

condensed DNA^{18,19}. On the contrary, with addition of zwitterionic species (which are more polarizable than water), Flock *et al.*²⁰ observed a resolubilization of DNA in the presence of multivalent ions (as condensating agents). Baigl and Yoshikawa²¹ found that zwitterionic species increased stability of coil states of a single DNA molecule, which undergoes a discontinuous phase transition between elongated coil and compact globule depending on the amounts of the second component and the multivalent ions.

To understand these mixture effects, relevance of the preferential solvation has been pointed out by experimental groups^{17,18,19} and by a theoretical group²². From our viewpoint, particularly important should be the ion-dipole interaction among charged particles and polar molecules²³, which gives rise to the solvation (hydration) shell composed of several solvent molecules (those of the more polar component in a mixture solvent) around each charged particle. The resultant solvation chemical potentials of ions typically much exceed the thermal energy $k_B T$ (per ion) and strongly depend on the composition in binary mixtures. It is decreased (increased) for hydrophilic (hydrophobic) ions with increasing the water composition in a mixture of water+ a less polar component. Furthermore, the degree of ionization of polymers can strongly depend on the composition. Very recently, including such solvation interactions, several theoretical groups have begun to investigate the ion effects in electrolytes with mixture solvents^{22,24,25,26,27,28}, polyelectrolytes¹⁵, and ionic surfactants at oil-water interfaces²⁹.

In this paper, we will demonstrate emergence of mesoscopically heterogeneous composition variations around a charged rod, which stem from the preferential solvation of charged particles. If they are hydrophilic, the water-like component is enriched near a rod, even when the polymer backbone is hydrophobic. In such complex situations, the original concept of the Manning-Oosawa counterion condensation is no longer available (or at least needs to be

modified) to understand the counterion distribution. As a byproduct, we will predict a first order phase transition between weakly and strongly ionized states of a rod, while the composition of the more polar component ϕ_B is small far from it. Here the ionization is assumed to be very weak for $\phi_B = 0$ and increase with increasing ϕ_B (or the solution dielectric constant). Our prediction is that the progress of ionization can occur as a discontinuous change. If a polymer chain is in an expanded state in the weakly ionized phase, it should be more expanded in the strongly ionized phase. It is analogous to the prewetting phase transition of fluids on a planar boundary wall^{30,31,32}.

In Section II, we will present a theory for one component solvents without and with salt, treating the degree of ionization α as a fluctuating variable. In Subsection IIIA, we will present a simple thermodynamic theory of the solvation shell formation at small composition ϕ_B of the more polar component. This effect takes place even at very small ϕ_B at strong preferential solvation. In Subsection IIIB, we will proceed to construct a Ginzburg-Landau theory for two component solvents at not small ϕ_B , which includes the degree of ionization α , the counterion density n_1 , and the composition ϕ as fluctuating variables. In Section IV, we will numerically examine these quantities in equilibrium for various parameters without salt. We will examine the first order phase transition between weakly and strongly ionized states of a rod. In Section V, we will summarize our main results. We will also discuss previous experimental findings of heterogeneities and mesophases induced by the preferential solvation in electropolytes and polyelectrolytes.

II. ROD IN ONE-COMPONENT SOLVENT

We consider an ionizable polymer chain with a long persistence length in a one-component solvent. Its shape is a rod or an expanded coil. Necklace-like globules are outside the scope of this work^{3,4,5,6,7,8}, which appear in poor solvents with increasing ionization. Assuming low density ions far from the polymer chain, we neglect the formation of dipole pairs and ion clustering⁴ (which is crucial at high ion densities in water) and the free energy contribution arising from the charge density fluctuations ($\propto \kappa^3$ with κ being the Debye-Hückel wave number)^{4,33}.

As a mathematical idealization, a polymer chain is treated as a cylinder with radius b and length L with $L \gg b$. The system is in a cylindrical cell with radius R with $R \gg b$. For an isolated polymer chain, the length L and the volume πLR^2 should be of the order of the persistence length and the chain volume, respectively. Thus $R^2 \sim R_G^3/L$, where R_G is the gyration radius. Neglecting the end effects we assume that all the quantities depend only on the distance r from the center of the rod.

A. Ginzburg-Landau free energy

Let the density of ionizable groups on a rod be σ_0 per unit length and the degree of ionization be α in the range $0 \leq \alpha \leq 1$. We assume homogeneity along the rod. Each ionized group has charge $-e$ and the counterions are monovalent. The charge density along the rod is given by $-e\sigma$ with

$$\sigma = \sigma_0 \alpha \quad (2.1)$$

per unit length. The ions including the counterions are distributed in the region $b < r < R$ and $0 < z < L$. Their densities are written as $n_i(r)$ and their charges are $Z_i e$ ($i = 1, 2, \dots$). In this work $n_1(r)$ denotes the density of the counterions from the rod plus the cations of the same species added as a strong salt. Then $Z_1 = 1$. The charge density in the region $b < r < R$ is expressed as

$$\rho = e \sum_i Z_i n_i, \quad (2.2)$$

where the summation is over all the mobile ions $i = 1, 2, \dots$. We assume the overall charge neutrality,

$$\int d\mathbf{r} \rho(r) = Le\sigma, \quad (2.3)$$

where $\int d\mathbf{r}(\dots) = 2\pi L \int_b^R dr r(\dots)$ is the integral in the cell outside the rod. In the present one-component case the dielectric constant ε is assumed to be a constant. The electric potential $\Phi(r)$ satisfies

$$\varepsilon \left(\frac{d^2}{dr^2} + \frac{1}{r} \frac{d}{dr} \right) \Phi = -4\pi\rho. \quad (2.4)$$

We impose the boundary condition on the electric field $E(r) = -d\Phi(r)/dr$ as

$$E(R) = 0. \quad (2.5)$$

That is, there is no surface charge on the outer surface. With the aid of Eqs.(2.3) and (2.5), integration of Eq.(2.4) in the region $b < r < R$ gives the boundary condition,

$$E(b) = -2e\sigma/\varepsilon b. \quad (2.6)$$

Our theory remains invariant with respect to the shift of the potential $\Phi(r) \rightarrow \Phi(r) + \text{const}$.

Hereafter we set the Boltzmann constant equal to unity. The Helmholtz free energy F of our system is divided in two parts as $F = F_0 + F_d$, where F_0 consists of the entropic and electrostatic contributions and F_d is the free energy of dissociation. They are written as^{11,12,13,14,15}

$$\frac{F_0}{T} = \int dr \left[\sum_i n_i (\ln(n_i v_0) - 1) + \frac{\varepsilon E^2}{8\pi T} \right], \quad (2.7)$$

$$\frac{F_d}{T} = L\sigma_0 [\alpha \ln \alpha + (1 - \alpha) \ln(1 - \alpha)] + L\Delta_0 \sigma. \quad (2.8)$$

In F_0 , the volume v_0 is taken to be independent of i , which is allowable without loss of generality³⁴. In F_d , $L\sigma_0$ is the total number of the ionizable groups and Δ_0 is the energy needed for ionization (see Eq.(2.15) for the dissociation constant in terms of Δ_0). The free ions can interact with polar segments on a chain, but such an interaction is neglected.

In equilibrium we minimize the grand potential $\Omega = F - \int d\mathbf{r} \sum_i \mu_i n_i$ under the charge neutrality condition Eq.(2.3), where μ_i ($i = 1, 2, \dots$) are appropriate constant chemical potentials. We thus minimize

$$\Omega = F - \int d\mathbf{r} \sum_i (\mu_i - T\lambda Z_i) n_i - T\lambda L\sigma \quad (2.9)$$

with respect to α and $n_i(r)$, where $T\lambda$ is the Lagrange multiplier. Without salt, however, we may redefine $\Delta_0 - \mu_1/T$ as Δ_0 to obtain $\mu_1 = 0$ and $\Omega = F$.

The electrostatic energy $F_e \equiv \int d\mathbf{r} \varepsilon E^2/8\pi$ in the cell changes with respect to small variations of σ , n_i , and ε as

$$\delta F_e = \int d\mathbf{r} \left[e\Phi \sum_i Z_i \delta n_i - \frac{E^2}{8\pi} \delta\varepsilon \right] - e\Phi(b) \delta\sigma, \quad (2.10)$$

where use has been made of Eqs.(2.4)-(2.6). In the present case $\delta\varepsilon = 0$, but will be nonvanishing for two component solvents. In terms of the normalized potential defined by

$$U(r) = e\Phi(r)/T, \quad (2.11)$$

the minimum conditions $\partial\Omega/\partial\alpha = \delta\Omega/\delta n_i = 0$ are rewritten as

$$\frac{\alpha}{1-\alpha} = \exp[\lambda + U(b) - \Delta_0], \quad (2.12)$$

$$n_i(r) = n_{0i} \exp[-Z_i(U(r) + \lambda)], \quad (2.13)$$

where $n_{0i} = v_0^{-1} e^{\mu_i/T}$ are constants. We notice that U and λ appear in the sum $U + \lambda$, so we are allowed to set $\lambda = 0$ by redefining $U + \lambda$ as U . Substitution of Eq.(2.13) into Eq.(2.4) yields the Poisson-Boltzmann equation. With these results Ω assumes a negative minimum expressed as

$$\frac{\Omega}{TL} = -\sigma + \sigma_0 \ln(1-\alpha) - \frac{F_e}{TL} - \frac{N_s}{L}, \quad (2.14)$$

where $N_s = \int d\mathbf{r} \sum_i n_i - \sigma L$ is the number of the ions added as a salt. In Eqs.(2.32) and (2.33) below, Ω will be calculated explicitly for $N_s = 0$ without salt.

As $r \rightarrow b$, we have $n_1(b) = n_{01} \exp[-U(b) - \lambda]$ for monovalent counterions. We thus obtain the mass action law (equation of ionization equilibrium),

$$\frac{\alpha}{1-\alpha} n_1(b) = K_0, \quad (2.15)$$

where K_0 is the dissociation constant for one component solvent,

$$K_0 = n_{01} e^{-\Delta_0} = v_0^{-1} e^{\mu_1/T - \Delta_0}. \quad (2.16)$$

Since Eq.(2.15) yields $\alpha = K_0/[K_0 + n_1(b)]$, α increases up to unity with decreasing $n_1(b)$. Note that K_0 is a measurable quantity and should be invariant with respect to the choice of v_0 in Eq.(2.7)³⁴.

B. Salt-free case

We first examine the salt-free case, where the Poisson-Boltzmann equation under the boundary conditions Eqs.(2.5) and (2.6) can be exactly solved^{9,35}. It is parameterized by the normalized line density $\ell_B\sigma$, called the Manning parameter, and the radius ratio R/b . Here $\ell_B = e^2/\varepsilon T$ is the Bjerrum length. The counterions tend to be localized around the rod for $\ell_B\sigma > 1$, but they are delocalized for $\ell_B\sigma < 1$. We examine how the degree of ionization α is determined for each given $\ell_B\sigma_0$.

1. Exact results and asymptotic behavior

It is known that $n_1(r) \propto r^{-2}$ and $E(r) \propto r^{-1}$ roughly hold for $r \gg b$. To seek the exact solution, it is convenient to introduce the dimensionless function,

$$F_1(r, \sigma) = 2\pi\ell_B r^2 n_1(r), \quad (2.17)$$

which behaves differently depending on whether $\sigma < \sigma^*$ or $\sigma > \sigma^*$ with σ^* being a critical line density,

$$\sigma^* = \ell_B^{-1}/(1 + M^{-1}). \quad (2.18)$$

Here we define the dimensionless parameter,

$$M = \ln(R/b), \quad (2.19)$$

which is assumed to be considerably larger than unity. The function $F_1(r, \sigma)$ depends on $\hat{r} \equiv r/R$ logarithmically as^{9,35}

$$\begin{aligned} \frac{F_1(r, \sigma)}{B^2} &= [\sinh(B \ln \hat{r} - \tanh^{-1} B)]^{-2} \quad (\sigma < \sigma^*) \\ &= [\sin(B \ln \hat{r} - \tan^{-1} B)]^{-2} \quad (\sigma > \sigma^*). \end{aligned} \quad (2.20)$$

The parameter B is the solution of the equation,

$$\begin{aligned} \frac{1 - \ell_B\sigma}{B} &= \coth[BM + \tanh^{-1} B] \quad (\sigma < \sigma^*) \\ &= \cot[BM + \tan^{-1} B] \quad (\sigma > \sigma^*), \end{aligned} \quad (2.21)$$

where we may set $B \geq 0$. At $\sigma = \sigma^*$, we have $B = 0$ and $F_1(r, \sigma^*) = (1 - \ln \hat{r})^{-2}$ for any $M > 0$. On the outer surface $r = R$, we set $\ln \hat{r} = 0$ in Eq.(2.20) to find that $F_1(R, \sigma)$ is equal to $1 - B^2$ for $\sigma < \sigma^*$ and to $1 + B^2$ for $\sigma > \sigma^*$. In Fig.1, we plot $F_1(r, \sigma)$ vs $\ln(r/b)$ for $\ell_B\sigma = 0.8, 1$, and 1.5 at $M = 6$. The corresponding values of B are 0.163, 0.225, and 0.361, respectively. The Manning parameter $\ell_B\sigma$ can be known from the relation

$$\int_0^{u_c} du F_1(r, \sigma) = \ell_B\sigma, \quad (2.22)$$

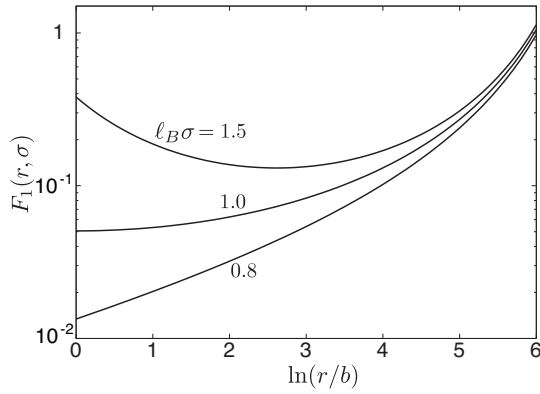


FIG. 1: $F_1(r, \sigma) = 2\pi\ell_B r^2 n_1(r)$ vs $\ln(r/b)$ on a logarithmic scale for $\ell_B\sigma = 0.8, 1$, and 1.5 for one component solvent without salt. The slope of the curve at $r/b = 1$ changes its sign at $\ell_B\sigma = 1$.

where $u = \ln(r/b)$ and $u_c = \ln(R/b)$. The normalized electric potential (2.11) is expressed as $U(r) = 2\ln(r/b) - \ln F_1(r, \sigma) + \text{const}$.

We need to express B in terms of $\ell_B\sigma$ from Eq.(2.21). We introduce a scaling variable q by

$$q = (\ell_B\sigma - 1)M. \quad (2.23)$$

At $\sigma = \sigma^*$ we have $q = -M/(1+M) \cong -1$. In the limit $|q| \ll 1$ the asymptotic expressions are

$$\begin{aligned} B &\cong 1 - \ell_B\sigma \quad (-q \gg 1), \\ &\cong \pi/M \quad (q \gg 1). \end{aligned} \quad (2.24)$$

On the outer surface $r = R$, we obtain the large M behavior $F_1(R, \sigma) \cong 1 - (1 - \ell_B\sigma)^2$ for $\ell_B\sigma < 1$ and $F_1(R, \sigma) \cong 1$ for $\ell_B\sigma > 1$ from Eq.(2.24). We may rewrite this result in terms of the osmotic pressure $\Pi = Tn_1(R)$ (at $r = R$ where the Maxwell stress vanishes). Let $n_p = \sigma/\pi R^2$ be the counterion density for the uniform distribution. At $r = R$ we have $n_1(R) = n_p F_1(R, \sigma)/2\ell_B\sigma$. In the limit $M \rightarrow \infty$, it follows the Manning limiting law for the osmotic pressure,

$$\begin{aligned} \Pi &\cong Tn_p(1 - \ell_B\sigma/2) \quad (\ell_B\sigma < 1) \\ &\cong Tn_p/2\ell_B\sigma \quad (\ell_B\sigma > 1), \end{aligned} \quad (2.25)$$

In the second line, Π saturates at $T/2\pi\ell_B R^2$ for σ larger than ℓ_B^{-1} , where a fraction of $1 - (\ell_B\sigma)^{-1}$ of the counterions are apparently localized around the rod (the Manning-Oosawa counterion condensation)^{1,2,3,4,5,6,7,8,9,10}.

2. Counterion density at $r = b$ and degree of ionization

In Fig.1, we show $F_1(r, \sigma)$ in Eq.(2.17) around $\ell_B\sigma = 1$. It changes most drastically at $r = b$ and most weakly at $r = R$. Here $F_1(b, \sigma) = 2\pi\ell_B b^2 n_1(b)$ is the normalized

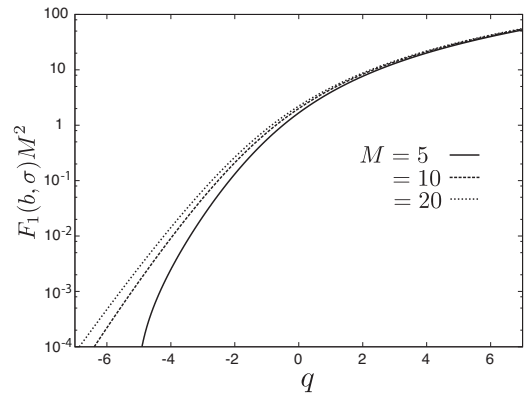


FIG. 2: Normalized counterion density on the rod surface $F_1(b, \sigma)M^2 = \pi\ell_B b^2 n_1(b)M^2$ vs $q = (\ell_B\sigma - 1)M$ on a semi-logarithmic scale for three values of $M = \ln(R/b)$ for one-component solvent without salt. As in Eq.(2.27) it tends to q^2 for $q \gg 1$ and decays as $4q^2 e^{2q}$ for $q \ll -1$ for large M .

counterion density at the rod surface. In the following, we calculate $F_1(b, \sigma)$ and α .

For $M \gg 1$, B is of order M^{-1} . In fact, on the right hand sides of Eq.(2.21), we may omit $\tanh^{-1} B$ in the first line and $\tan^{-1} B$ in the second line to obtain

$$\begin{aligned} q &\cong -BM/\tanh(BM) \quad (q < -1), \\ &\cong -BM/\tan(BM) \quad (q > -1). \end{aligned} \quad (2.26)$$

For $q \ll -1$ we have $BM \cong -q$. For $q > -1$, BM monotonically increases from 0 up to π with increasing q from -1 . These limiting relations are consistent with Eq.(2.24) for $|q| \gg 1$. We recognize that the scaled quantity $F_1(r, \sigma)M^2$ tends to a function of r/R and q as $M \rightarrow \infty$. At $r = b$, it is given by $4q^2 e^{2q}$ for $q \ll -1$ and by q^2 for $q \gg 1$. Thus,

$$\begin{aligned} F_1(b, \sigma) &\cong 4(\sigma\ell_B - 1)^2 e^{-2(1-\ell_B\sigma)M} \quad (-q \gg 1), \\ &\cong (\sigma\ell_B - 1)^2 \quad (q \gg 1), \end{aligned} \quad (2.27)$$

while $F_1(b, \sigma) \sim M^{-2}$ for $|q| \sim 1$. Figure 2 displays $F_1(b, \sigma)M^2$ vs q for $M = 5, 10$, and 20 , where the curves are numerically obtained from Eqs.(2.20) and (2.21). It is 1.67 for $M = 5$ and 2.22 for $M = 20$ at $q = 0$, while it is 7.64 for $M = 5$ and 8.80 for $M = 20$ at $q = 2$. Thus the second line of Eq.(2.27) is a good approximation in the region $q > 0$ even for $M = 5$. However, for $q < -2$, $F_1(b, \sigma)M^2$ is very small (< 0.1), where the M dependence of the curves is not small.

We now calculate α from Eqs.(2.15), (2.20), and (2.21). In Fig. 3, plotted are numerical results of α , $F_1(b, \sigma)$, and Π/Tn_p for $\ell_B\sigma_0 = 0.8$ (left) and 1.5 (right). They are functions of the normalized dissociation constant,

$$A = 2\pi\ell_B b^2 K_0. \quad (2.28)$$

In terms of A , Eq.(2.15) is rewritten as

$$\alpha F_1(b, \sigma) = (1 - \alpha)A. \quad (2.29)$$

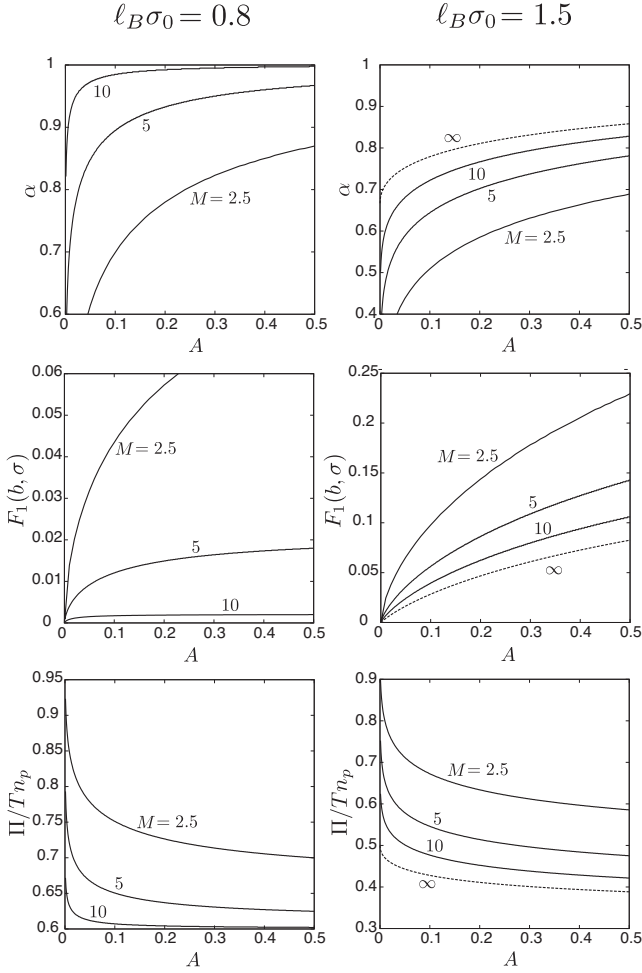


FIG. 3: Degree of ionization α (top), normalized counterion density $F_1(b, \sigma)$ on the rod surface (middle), and osmotic pressure Π at $r = R$ divided by $Tn_p = T\sigma/\pi R^2$ (bottom) as functions of the normalized dissociation constant A in Eq.(2.28) for $\ell_B \sigma_0 = 0.8$ (left) and 1.5 (right) without salt.

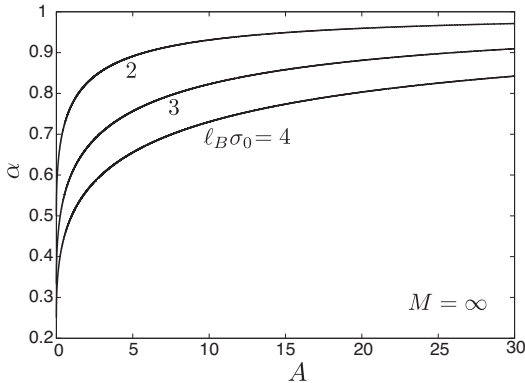


FIG. 4: Degree of ionization α vs A for $\ell_B \sigma_0 = 2, 3, 4$ obtained from the asymptotic equation (2.31) in the limit $R \rightarrow \infty$. Here $\alpha \rightarrow 1/\ell_B \sigma_0$ as $A \rightarrow 0$, while $\alpha \rightarrow 1$ for $A \gg 1$.

For $(1 - \ell_B \sigma)M \gg 1$ the first line of Eq.(2.27) gives

$$(1 - \ell_B \sigma_0 \alpha)^2 \alpha \cong \frac{A}{4} (R/b)^{2(1 - \ell_B \sigma_0 \alpha)} (1 - \alpha), \quad (2.30)$$

which depends on R/b anomalously. As $A \rightarrow 0$, the linear growth $\alpha \cong c_1 A \ll 1$ follows with $c_1 = (R/b)^2/4$, so α increases very steeply since $c_1 \gg 1$. Then there are two cases. (i) If $\sigma_0 < \ell_B^{-1}$, α quickly approaches unity with increasing A as $\alpha \cong 1 - c_2/A \rightarrow 1$ with $c_2 = 4(1 - \ell_B \sigma_0)^2 (b/R)^{2(1 - \ell_B \sigma_0)}$ for $A \gtrsim c_1^{-1}$, as in the left panels in Fig.3. In this case $\Pi/Tn_p \rightarrow 1 - \ell_B \sigma_0/2$ From Eq.(2.25). (ii) In the other case $\sigma_0 > \ell_B^{-1}$, α quickly exceeds $(\ell_B \sigma_0)^{-1}$ at $A \sim (b/R)^2 \ll 1$.

We then consider the case $(\ell_B \sigma - 1)M \gg 1$, where the second line of Eq.(2.27) gives the asymptotic equation independent of R/b ,

$$(\ell_B \sigma_0 \alpha - 1)^2 \alpha \cong A(1 - \alpha). \quad (2.31)$$

This cubic equation of α yields a unique solution in the range $(\ell_B \sigma_0)^{-1} < \alpha < 1$. Namely, $\alpha \rightarrow (\ell_B \sigma_0)^{-1} < 1$ as $A \rightarrow 0$, while $\alpha \rightarrow 1$ with increasing A . In Fig. 4, we show this limiting α obtained from Eq.(2.31) as a function of A for $\ell_B \sigma_0 > 1$, where the increase of α from 0 to $(\ell_B \sigma_0)^{-1}$ in the narrow region $0 < A \lesssim (b/R)^2$ is not shown.

3. Free energy and effective polymer-solvent interaction

In equilibrium without salt, the grand potential Ω in Eq.(2.14) consists of three negative parts as

$$\Omega/TL = -2\sigma - \ell_B^{-1} \mathcal{F}_e(\ell_B \sigma) + \sigma_0 \ln(1 - \alpha), \quad (2.32)$$

where $F_e = TL(\sigma + \ell_B^{-1} \mathcal{F}_e)$. The exact expression for the scaling function $\mathcal{F}_e(s)$ was derived by Naji and Netz¹⁰. See the appendix. For large M we approximate it as

$$\begin{aligned} \mathcal{F}_e(s) &\cong s^2 M + 2 \ln \left[\frac{2 - 2s}{2 - s} + M^{-1} \right] \quad (q < -1) \\ &\cong M + 2 \ln(s - 1 + M^{-1}) \quad (q > -1), \end{aligned} \quad (2.33)$$

where $s = \ell_B \sigma$ and $q = M(s - 1)$. We introduce M^{-1} on the right hand sides to avoid the logarithmic divergence at $s = 1$. (i) For small $\ell_B \sigma \ll M^{-1}$ the electrostatic part is negligible and $\Omega/TL \cong -\sigma + \sigma_0 \ln(1 - \alpha)$. (ii) On the other hand, for $\ell_B \sigma - 1 \gg M^{-1}$ and $\ell_B \sigma \ll M$, we find

$$F_e \cong TL \ell_B^{-1} M, \quad (2.34)$$

$$\Omega/TL \cong -\ell_B^{-1} M + \sigma_0 \ln(1 - \alpha). \quad (2.35)$$

The electrostatic energy is nearly equal to that of a charged rod at $\sigma = \ell_B^{-1}$ without screening. This result suggests that a fraction of $1 - (\ell_B \sigma)^{-1}$ of the counterions are localized around the rod, as well as the osmotic pressure behavior in Eq.(2.25).

Polymer chains in water are often hydrophobic without ionization but can be hydrophilic with ionization^{5,7,8}.

This means that the polymer-solvent interaction parameter, written as χ_{ps} , is effectively decreased upon ionization. Its decrease $\Delta\chi_{ps}$ may be defined as follows. In the Flory-Huggins free energy density of polymer solutions, the interaction part is written as $Tv_0^{-1}\chi_{ps}\phi_p$ for small polymer volume fraction ϕ_p , where v_0 is the solvent volume. We map our polyelectrolyte system to a neutral polymer system. In the present case, the polymer volume is $\pi b^2 L$ in the total volume $V = \pi LR^2$ so that $\phi_p = (b/R)^2$. We set

$$Tv_0^{-1}\Delta\chi_{ps}\phi_p = \Omega/V + \Pi. \quad (2.36)$$

Without salt we have $\Pi = Tn_1(R)$ and

$$\Delta\chi_{ps} = \frac{v_0}{\pi b^2} \left[\frac{\Omega}{TL} + \pi R^2 n_1(R) \right], \quad (2.37)$$

where the first term in the brackets is given by Eq.(2.32) and the second term in the brackets is $F_1(R, \sigma)/2\ell_B$ from Eq.(2.17). For small $\ell_B\sigma \ll M^{-1}$ we have $\Delta\chi_{ps} \cong (v_0/\pi b^2 \ell_B)\sigma_0 \ln(1 - \alpha)$. For $\ell_B\sigma - 1 \gg M^{-1}$ and $\ell_B\sigma \ll M$, we have $\Delta\chi_{ps} \cong (v_0/\pi b^2)\Omega/TL$, where Ω is given by Eq.(2.34). The negativity of $\Delta\chi_{ps}$ indicates an increase of the solvent quality upon ionization.

C. Two species of free ions

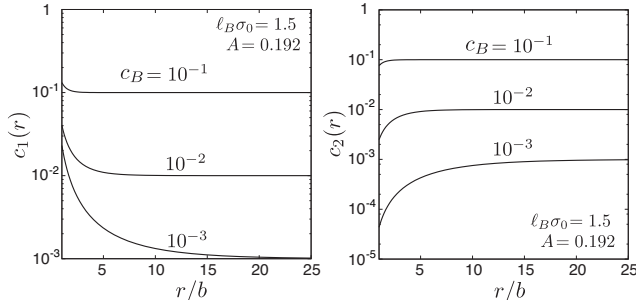
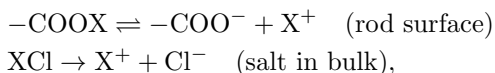


FIG. 5: Normalized density of cations $c_1(r) = \ell_B b^2 n_1(r)$ (left) and anions $c_2(r) = \ell_B b^2 n_2(r)$ (right) vs r/b at $\ell_B\sigma_0 = 1.5$ and $A = 0.192$. The salt density is given by $c_B = \ell_B b^2 n_B = 10^{-1}, 10^{-2}$ and 10^{-3} .

We add a small amount of a monovalent salt, which is completely dissociated into cations and anions. For simplicity, we assume that the cations from the salt are of the same species as the counterions from the rod. For example, we suppose the chemical reactions:



where $\text{X}=\text{H}$ or Na . The cation and anion densities are denoted by n_1 and n_2 , respectively. Here we treat the anion density at $r = R$ as a control parameter and write

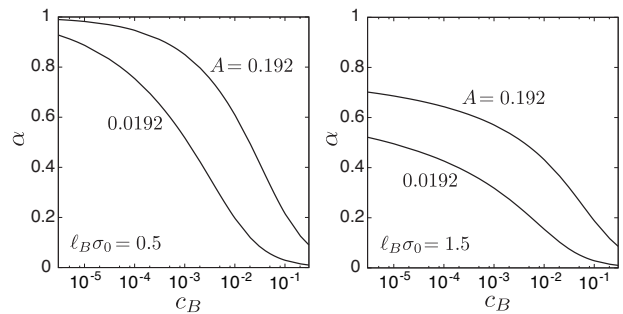


FIG. 6: Degree of ionization α as a functions of salt concentration $c_B \ell_B b^2 n_B$ on a semi-logarithmic scale for $A = 0.192$ and 0.0192 . Here $\ell_B\sigma_0 = 0.5 < 1.0$ (left) and $\ell_B\sigma_0 = 1.5 > 1.0$ (right).

it as n_B . In this case, the electric field created by the positive charges on the rod is screened for $r > k_D^{-1}$, where

$$k_D = (8\pi\ell_B n_B)^{1/2} \quad (2.38)$$

is the Debye wave number far from the rod. For $r \gg k_D^{-1}$, the system is homogeneous with $n_1(r) \cong n_2(r)$. If $R \gg k_D^{-1}$, we obtain the results in the limit $R \rightarrow \infty$. By setting $\Phi(\infty) = 0$, we may write the ion densities as $n_1 = n_B e^{-U}$ and $n_2 = n_B e^U$ with $U = e\Phi/T$, where $n_1(\infty) = n_2(\infty) = n_B$. We rewrite the Poisson-Boltzmann equation as

$$\left(\frac{d^2}{dr^2} + \frac{1}{r} \frac{d}{dr} \right) U = k_D^2 \sinh U, \quad (2.39)$$

The boundary condition is given by Eq.(2.5) at $r = b$.

We numerically solved the Poisson-Boltzmann equation Eq.(2.39) and the ionization equation Eq.(2.15) to obtain the equilibrium $n_1(r)$, $n_2(r)$, and α . The normalized salt density at infinity is written as $c_B = \ell_B b^2 n_B$. In Fig. 5, we plot the normalized ion densities,

$$\begin{aligned} c_1(r) &= \ell_B b^2 n_1(r), \\ c_2(r) &= \ell_B b^2 n_2(r), \end{aligned} \quad (2.40)$$

where we set $\ell_B\sigma_0 = 1.5$ and $A = 0.192$. Here $c_1(r)$ increases and $c_2(r)$ decreases near the rod. In Fig. 6, we show α as a function of c_B for $\ell_B\sigma_0 = 0.5$ and 1.5 . We find that α decreases with increasing the salt concentration c_B . This is consistent with Fig. 5, where $n_1(b)$ becomes larger with increasing c_B . We also find $\alpha \rightarrow 1$ as $c_B \rightarrow 0$ for $\ell_B\sigma_0 = 0.5 < 1$, while α does not approach unity as $c_B \rightarrow 0$ for $\ell_B\sigma_0 = 1.5 > 1$. This is consistent with the behavior of α in the limit $M \rightarrow \infty$ in the salt-free case discussed in the previous subsection. In the limit $c_B \rightarrow 0$ (with $R = \infty$), α approaches unity for $\ell_B\sigma_0 < 1.0$ (though this limiting behavior is not seen for $A = 0.0192$ in the left panel), while it tends to a constant in the range $[(\ell_B\sigma_0)^{-1}, 1]$ for $\ell_B\sigma_0 > 1.0$ as can be seen in the right panel.

In summary, with increasing the salt density, the degree of ionization α is reduced and the electrostatic interaction is screened. Experimentally, with addition of salt, the highly expanded polyelectrolyte coils have been observed to shrink, eventually resulting in precipitation of the chains (phenomenon known as "salting out" of polyelectrolytes⁵).

III. ROD IN TWO COMPONENT SOLVENT

We next consider a charged rod in a nearly incompressible two component solvent such as a mixture of water+alcohol or water+an organic solvent in the same geometry as in the one-component case. The volume fraction of the water-like component is $\phi(r)$ and that of the less polar component is $1 - \phi(r)$. We suppose a polymer chain with a hydrophobic backbone (like polystyrene) and a small fraction of ionizable groups. It is soluble in the second (less polar) component with little dissociation, but ionization increases with addition of the first (water-like) component. That is, $\alpha \ll 1$ for $\phi = 0$, but α increases with addition of the first component.

For simplicity, the molecular volumes of the two components (the inverse densities of the pure components) are assumed to be given by a common volume $v_0 = a^3$, which may be equated with v_0 in Eq.(2.7). Hence ϕ will also be called the composition. We assume small sizes of the ions and neglect their volume fraction. As in Section 1, $n_1(r)$ denotes the density of the counterions plus the cations of the same species added as a salt.

A. Water adsorption at small bulk composition

With addition of water, we first need to consider the formation of solvation (or hydration) shells composed of several water molecules around hydrophilic charged particles²³. We mention an experiment using a coextraction method by Osakai and Ebina³⁶. In water-nitrobenzene(Nr) in two phase coexistence, they measured the number of hydrating water molecules around ions in a Nr-rich region at room temperatures. The water number per ion in the Nr-rich phase was estimated to be 4 for Na^+ , 6 for Li^+ , and 15 for Ca^{2+} , while it was nearly zero for hydrophobic ions. Their experiment demonstrates strong binding of water molecules to hydrophilic ions even at small water compositions in a mixture solvent.

We present a simple theory of water adsorption to the ionized monomers³⁷. The system is in the cylindrical cell $b < r < R$ and $0 < z < L$. We assume that each solvation shell can consist of ν water molecules with the binding energy Tw_ν , where $\nu = 1, \dots, Z$ with Z being the maximum number. Let the number of the ionized monomers be $N_I = L\sigma$ and the number of the ν -clusters composed of ν water molecules around a hydrophilic charged monomer be $\beta_\nu N_I$. The total number of the hydrated

ionized monomers is then βN_I with

$$\beta = \sum_{\nu=1}^K \beta_\nu < 1. \quad (3.1)$$

The fractions β_ν are determined by minimization of the free energy of the form,

$$\begin{aligned} \frac{F_s}{T} = & N_0 \phi_B (\ln \phi_B - 1) + N_I (1 - \beta) \ln(1 - \beta) \\ & + N_I \sum_{\nu=1}^K \beta_\nu (\ln \beta_\nu - w_\nu), \end{aligned} \quad (3.2)$$

where $N_0 = V/v_0$ with $V = \pi(R^2 - b^2)L$ being the total volume occupied by the solvent. The conservation of the water molecules yields

$$N_0 \phi_B + N_I \sum_{\nu=1}^K \nu \beta_\nu = N_0 \phi_B^0, \quad (3.3)$$

where ϕ_B^0 is the water volume fraction without adsorption. The minimization condition $\partial F_s / \partial \beta_\nu = 0$ under Eq.(3.3) yields

$$\beta_\nu = (1 - \beta) \phi_B^\nu e^{w_\nu}. \quad (3.4)$$

where Eq.(3.1) gives

$$\beta = 1 - 1 / \left[1 + \sum_{\nu=1}^K \phi_B^\nu e^{w_\nu} \right]. \quad (3.5)$$

For $N_I \ll N_0$ or for $R \gg b$, we may set $\phi_B - \phi \ll \phi$ even if β approaches unity. We then calculate the excess free energy $\Delta F_s = F_s - T N_0 \phi_B^0 (\ln \phi_B^0 - 1)$ due to the water adsorption. Some calculations give

$$\begin{aligned} \frac{\Delta F_s}{T} = & N_0 \phi_B^0 \ln(\phi_B / \phi_B^0) + N_I [\phi_B^0 - \phi_B + \ln(1 - \beta)] \\ \cong & -N_I \ln \left[1 + \sum_{\nu=1}^K \phi_B^\nu e^{w_\nu} \right]. \end{aligned} \quad (3.6)$$

Here we set $\ln(\phi_B / \phi_B^0) \cong \phi_B / \phi_B^0 - 1$ in the first line to obtain the second line for $N_I \ll N_0$.

The formation of solvation shells around the counterions may be analyzed in the same manner. Let Tw'_ν be the binding energy of ν -clusters of hydrating water molecules. If the counterions are monovalent, we find the free energy decrease in the same form as that in Eq.(3.6) with w_ν being replaced by w'_ν . Supposing a sufficiently small water density outside the solvation shells, we may use the results of one-component solvents in Section 2 if Δ_0 is replaced by or renormalized as

$$\tilde{\Delta}_0 = \Delta_0 - \ln \left\{ \left[1 + \sum_{\nu=1}^K \phi_B^\nu e^{w_\nu} \right] \left[1 + \sum_{\nu=1}^{K'} \phi_B^\nu e^{w'_\nu} \right] \right\}. \quad (3.7)$$

The dissociation constant K_0 in Eq.(2.16) is changed as

$$\begin{aligned} \tilde{K}_0 &= n_{01}e^{-\tilde{\Delta}_0} \\ &= K_0 \left[1 + \sum_{\nu=1}^K \phi_B^\nu e^{w_\nu} \right] \left[1 + \sum_{\nu=1}^{K'} \phi_B^\nu e^{w'_\nu} \right], \end{aligned} \quad (3.8)$$

The degree of ionization α is increased, since A should be replaced by $\tilde{A} = 2\pi\ell_B b^2 \tilde{K}_0 > A$ in Eq.(2.29). If the maximum of w_ν/ν and w'_ν/ν is denoted by w_s , ionization enhancement occurs for

$$\phi_B \gg e^{-w_s}, \quad (3.9)$$

due to the solvation shell formation. If $w_s \gg 1$, Eq.(3.9) can be satisfied even for small ϕ_B .

B. Ginzburg-Landau theory for concentrated water composition

For not very small ϕ_B , the water composition $\phi(r)$ varies on mesoscopic scales longer than a . To describe such situations, we present a Ginzburg-Landau theory with the gradient free energy of the composition³³.

1. Free energy including solvation interaction

The total free energy is composed of three parts as $F = F_0 + F_d + \Delta F$, where F_0 is given in Eq.(2.7) and F_d in Eq.(2.8). Notice that Δ_0 in Eq.(2.7) should be replaced by $\tilde{\Delta}_0$ in Eq.(3.7) to account for the solvation shell formation. Hereafter we will redefine Δ_0 as the right hand side of Eq.(3.7). Namely, Δ_0 in the following is the renormalized one unless confusion may occur.

Assuming the homogeneity along the rod, we write the additional contribution ΔF in the form,

$$\begin{aligned} \frac{\Delta F}{T} &= \int dr \left[\frac{f_0(\phi)}{T} + \frac{C}{2} |\nabla\phi|^2 - \sum_i g_i n_i \phi \right] \\ &\quad - 2\pi b L \gamma \phi_s - L \Delta_1 \sigma_0 \alpha \phi_s. \end{aligned} \quad (3.10)$$

The space integral is in the cell, $b < r < R$ and $0 < z < L$. The free energy density $f_0(\phi)$ is taken to be the Bragg-Williams form,

$$f_0 = \frac{T}{v_0} [\phi \ln \phi + (1 - \phi) \ln(1 - \phi) + \chi \phi(1 - \phi)], \quad (3.11)$$

where χ is the interaction parameter dependent on T and its mean-field critical value is 2 in the absence of ions. The coefficient C of the gradient part is a positive constant of order a^{-1} and will be taken to be $3a^{-1}$ in our numerical analysis. The coupling terms ($\propto g_i$) arise from the ion-dipole interactions among the ions and the polar solvent molecules. In the second line of Eq.(3.10), the term proportional to γ arises from the short-range interaction between the rod surface and

the solvent molecules³⁰, while the term proportional to Δ_1 represents the solvation interaction between the surface charge with line density $\sigma = \sigma_0 \alpha$ and the solvent molecules. Hereafter,

$$\phi_s = \phi(b) \quad (3.12)$$

is the surface value of the composition (outside the solvation shells under the condition (3.9)). These molecular interactions of the rod are characterized by the two constants γ and Δ_1 , which can be either negative or positive.

In F_0 in Eq.(2.7), the dielectric constant ε is assumed to depend on the composition in the linear form³⁸,

$$\varepsilon(\phi) = \varepsilon_0 + \varepsilon_1 \phi, \quad (3.13)$$

where $\varepsilon_0 + \varepsilon_1$ is the dielectric constant of the first component and ε_0 is that of the second component. Thus $\varepsilon(\phi)$ is inhomogeneous. The electric potential $\Phi(r)$ satisfies

$$\frac{1}{r} \frac{d}{dr} r \varepsilon(\phi) \frac{d}{dr} \Phi = -4\pi\rho, \quad (3.14)$$

under the boundary conditions,

$$E(b) = -2e\sigma/\varepsilon(\phi_s)b \quad (3.15)$$

and $E(R) = 0$ for the electric field $E(r) = -d\Phi/dr$. Using σ we integrate the Poisson equation (3.14) as

$$\frac{d\Phi(r)}{dr} = \frac{2}{r\varepsilon(\phi)} \left[e\sigma - 2\pi \int_b^r dr' r' \rho(r') \right]. \quad (3.16)$$

2. Minimization of the grand potential

We minimize the grand potential Ω defined as in Eq.(2.9) with $F = F_0 + F_d + \Delta F$. The counterparts of Eqs.(2.12) and (2.13) read

$$\frac{\alpha}{1 - \alpha} = \exp[\lambda + U(b) - \Delta_0 + \Delta_1 \phi_s], \quad (3.17)$$

$$n_i(r) = n_{0i} \exp[-Z_i(\lambda + U(r)) + g_i \phi(r)], \quad (3.18)$$

where $n_{0i} = v_0^{-1} e^{\mu_i/T}$. As in Section 1, we may set $\lambda = 0$ without loss of generality. From these equations the mass action law follows as

$$\frac{\alpha}{1 - \alpha} n_1(b) = K(\phi_s). \quad (3.19)$$

The dissociation constant $K(\phi_s)$ depends on the surface composition ϕ_s as

$$K(\phi_s) = \tilde{K}_0 e^{(\Delta_1 + g_1)\phi_s}. \quad (3.20)$$

See Eq.(3.8) for \tilde{K}_0 . With increasing ϕ_s , $K(\phi_s)$ increases (decreases) for positive (negative) $\Delta_1 + g_1$. We are not aware of experimental data on the composition dependence of α for polymers in mixture solvents. On the other hand, strong composition dependence has been reported in dissociation of weak acids in various aqueous mixtures (see the item (vi) in the summary section)^{39,40}.

The functional derivative $h = \delta F / \delta \phi$ at fixed n_i and α is the chemical potential difference of the two components divided by v_0 and is homogeneous in equilibrium. From Eqs.(2.10) and (3.10) we obtain

$$h = f'_0(\phi) - TC\nabla^2\phi - T \sum_i g_i n_i - \frac{\varepsilon_1}{8\pi} E^2. \quad (3.21)$$

where $f'_0(\phi) = \partial f_0(\phi) / \partial \phi$ and $E = -d\Phi/dr$. In equilibrium h is a homogeneous constant.

With these results it is convenient to redefine the grand potential as

$$\Omega = F - \int dr \left[\sum_i \mu_i n_i + f_0(\phi_B) + h(\phi - \phi_B) \right], \quad (3.22)$$

where $\phi_B = \phi(R)$ is the value of ϕ at $r = R$. As in Eq.(2.14) some calculations give

$$\begin{aligned} \frac{\Omega}{TL} &= 2\pi \int_b^R dr r \left[\frac{1}{T} \hat{f}_0(\phi) + \frac{C}{2} \phi'^2 \right] - 2\pi b \gamma \phi_s \\ &\quad - \sigma + \sigma_0 \ln(1 - \alpha) - \frac{F_e}{TL} - \frac{N_s}{L}. \end{aligned} \quad (3.23)$$

In the first line we write $\phi' = d\phi/dr$ and define

$$\hat{f}_0(\phi) = f_0(\phi) - f_0(\phi_B) - h(\phi - \phi_B). \quad (3.24)$$

The second line is of the same form as the right hand side of Eq.(2.14) with N_s being the number of ions from salt.

Small variations of ϕ , α , and n_i yield an incremental change in Ω , written as $\delta\Omega$. With the equilibrium conditions (3.14), (3.17), (3.18), and (3.21), its linear terms proportional to $\delta\alpha$ and δn_i vanish. There remain surface parts of the form,

$$\begin{aligned} \frac{\delta\Omega}{LT} &= 2\pi C[(r\phi'\delta\phi)_{r=R} - (r\phi'\delta\phi)_{r=b}] \\ &\quad - (2\pi b\gamma + \Delta_1\sigma)\delta\phi(b). \end{aligned} \quad (3.25)$$

In this paper we set $\delta\Omega = 0$ for any boundary variations $\delta\phi(b)$ and $\delta\phi(R)$ for simplicity. Then we obtain

$$\phi'(R) = 0, \quad (3.26)$$

$$C\phi'(b) = -\gamma - (\Delta_1/2\pi b)\sigma, \quad (3.27)$$

which are the boundary conditions on ϕ in solving the equation $h = \text{const.}$ in Eq.(3.21). In our theory the condition at $r = b$ in Eq.(3.27) depends on σ . For positive (negative) $\gamma + \Delta_1\sigma/2\pi b$, the first component tends to be attracted to (repelled from) the rod. A similar boundary condition has been used in the gradient theory of the wetting transition on a planar wall³⁰.

We comment on the gradient free energy with a constant coefficient C in Eq.(3.10). It is usually derived from the gradient expansion of the two body van der Waals interactions and is justified near the critical point. In the following, however, we will present numerical results in the composition range $0.15 < \phi_B < 0.53$ far from the

critical point, imposing the boundary condition (3.27) in the gradient theory, where ϕ_B is the composition far from the rod. When the rod radius b is of order a and ϕ changes steeply around the rod, a density functional theory without the gradient expansion should yield more reliable results^{31,32}.

3. Solvation interaction

In the original Born theory⁴¹, the solvation chemical potential was given by $\mu_{\text{sol}}^i(\phi) = Z_i^2 e^2 / 2\varepsilon(\phi) R_i$, where $Z_i e$ is the charge of ion species i , $\varepsilon(\phi)$ is the solvent dielectric constant dependent on ϕ , and R_i is a microscopic length called the Born radius. However, this formula is a crude approximation and is not applicable to hydrophobic ions. In this paper we assume the form

$$\mu_{\text{sol}}^i(\phi) = \mu_{\text{sol}}^i(0) - T g_i \phi. \quad (3.28)$$

The solvation contribution to the free energy density is given by $\sum_i \mu_{\text{sol}}^i(\phi) n_i$, yielding the terms proportional to g_i on the right hand side of Eq.(3.10). For a mixture of water and oil, for example, $T g_i$ is the difference of the solvation chemical potential in oil and that in water. Therefore, $g_i > 0$ for hydrophilic ions and $g_i < 0$ for hydrophobic ions in aqueous mixture solvents.

We should note that $T g_i$ may be equated with the so-called Gibbs transfer energy^{36,42} (per ion) from oil to water (in strong segregation) in electrochemistry. The latter experimental values are available for various ions in water+nitrobenzene mixtures at $T \sim 300\text{K}$ ^{36,42}, yielding $g_i \sim 15$ for monovalent ions such as Na^+ and Br^- and $g_i \sim -15$ for hydrophobic tetrarphenylborate BPh_4^- . For water+alcohol mixtures, $|g_i|$ should not be smaller, since the dielectric constant of nitrobenzene is 35 and that of alcohol is smaller (24 for ethanol). Thus the solvation coupling in aqueous mixtures is typically very strong.

In the free energy density (3.10) we introduce the interaction between the ionized monomers and the solvent molecules ($\propto \Delta_1 \alpha \phi_s$). However, we neglect the interaction between the mobile ions and the uncharged monomers, which was introduced in our previous paper¹⁵ and can be important for polar monomers.

4. Behavior of composition deviation

The composition $\phi(r)$ tends to a constant ϕ_B far from the rod. We treat ϕ_B as a control parameter. With a salt added, this behavior is obvious if the Debye screening length k_D^{-1} is shorter than the system radius R and longer than the correlation length ξ . In such a case Eq.(3.21) gives $\phi(r) - \phi_B \propto e^{-k_D r}$ far from the rod.

Without salt, however, the decay turns out to be algebraic. To show it, we linearize Eq.(3.21) with respect to the composition deviation $\delta\phi = \phi - \phi_B$ to obtain

$$(1 - \xi^2 \nabla^2) \delta\phi = \chi_s g_1 n_1 + \frac{\chi_s \varepsilon_1}{8\pi T} E^2, \quad (3.29)$$

where we assume $|\delta\phi| \ll \phi_B$ at any r . We define the correlation length ξ and the susceptibility χ_s as

$$\xi = [TC/f_0''(\phi_B)]^{1/2}, \quad (3.30)$$

$$\chi_s = T/f_0''(\phi_B) = \xi^2/C, \quad (3.31)$$

where $f_0''(\phi) = T[1/\phi(1-\phi) - 2\chi]/v_0$ from Eq.(3.11). In this paper, we set $C = 3/a$; then, $\chi_s \sim a\xi^2$. The length ξ remains of order a away from the criticality, while it grows near the criticality.

The two terms on the right hand side of Eq.(3.29) roughly behave as r^{-2} from the results for one-component solvent. That is, if $F_1 = 2\pi\ell_{B0}r^2n_1(r)$ in Eq.(2.17) (or in Eq.(3.39) below) is of order unity, the two terms are of order $\chi_s g_1/2\pi\ell_{Bb}r^2$ and $\chi_s \varepsilon_1/2\pi\varepsilon_0\ell_{Bb}r^2$, respectively. We define two Bjerrum lengths as

$$\begin{aligned} \ell_{B0} &= e^2/\varepsilon_0 T, \\ \ell_{Bb} &= e^2/\varepsilon_B T, \end{aligned} \quad (3.32)$$

at $\varepsilon = \varepsilon_0$ and $\varepsilon = \varepsilon(\phi_B) = \varepsilon_B$, respectively. Thus $\ell_{Bb} = \ell_{B0}/(1 + \varepsilon_1\phi_B/\varepsilon_0)$. Furthermore, we are interested in the strong solvation case $g_1 \gg 1$ with $\varepsilon_1/\varepsilon_0 \sim 1$ in this paper, where the first term dominates over the second in the right hand side of Eq.(3.29). Then $\delta\phi(r)$ decays for $r - b \gtrsim \xi$ as

$$\delta\phi(r) \sim (g_1 a \xi^2 / 2\pi\ell_{Bb}) r^{-2}. \quad (3.33)$$

Here we are assuming $|\delta\phi| \lesssim \phi_B$, which holds even for $r \sim \xi$ if $g_1 a / 2\pi\ell_{Bb} \lesssim 1$.

5. Effective rod charge in the salt-free case

For large r far from the rod, $\phi(r)$ tends to a constant ϕ_B and $n_1(r)$ obeys the nonlinear Poisson-Boltzmann equation even in the salt-free case. We introduce a characteristic length r_c in the range $b < r_c \ll R$. For r larger than r_c , we may set $\varepsilon(\phi) \cong \varepsilon_B$ with $\varepsilon_B = \varepsilon(\phi_B)$ and the potential $\Phi(r)$ obeys

$$-\varepsilon_B \nabla^2 \Phi \cong 4\pi e n_0 \exp(-e\Phi/T), \quad (3.34)$$

where we set $Z_1 = 1$ and $n_0 = n_{01}e^{-\lambda}$. We compare $\Phi(r)$ and $n_1(r)$ in our system approximately obeying Eq.(3.34) far from the rod and those obtained as the solution of the nonlinear Poisson-Boltzmann equation,

$$-\varepsilon_B \nabla^2 \Phi_{PB} = 4\pi e n_1^{PB}, \quad (3.35)$$

where $n_1^{PB}(r) = n_0 \exp(-e\Phi_{PB}(r)/T)$ is the corresponding counterion density. We set $\Phi_{PB}(R) = 0$ at $r = R$ and impose the boundary condition on $\Phi_{PB}(r)$ at $r = r_c$ as

$$\Phi_{PB}'(r_c) = \Phi'(r_c), \quad (3.36)$$

where $\Phi_{PB}'(r) = d\Phi_{PB}(r)/dr$ and $\Phi'(r) = d\Phi(r)/dr$. From Eq.(3.35) $\Phi(r) \cong \Phi_{PB}(r)$ and $n_1(r) \cong n_1^{PB}(r)$ far

from the rod $r > r_c$, but significant differences can arise in the region $r < r_c$.

In terms of Φ_{PB} we define the effective charge density σ_{eff} on the rod by

$$\sigma_{\text{eff}} = \varepsilon_B b \Phi_{PB}'(b) / 2e. \quad (3.37)$$

From Eq.(2.6) the real charge density σ is given by $\sigma = \varepsilon(\phi_s) b \Phi'(b) / 2e$. From Eqs.(3.16), (3.34), and (3.35) the apparent excess charge density $\Delta\sigma = \sigma_{\text{eff}} - \sigma$ on the rod is expressed as

$$\begin{aligned} \Delta\sigma &= 2\pi n_0 \int_b^{r_c} dr r [e^{-e\Phi(r)/T} - e^{-e\Phi_{PB}(r)/T}] \\ &= \frac{1}{\ell_{B0}} \int_0^{u_c} du [F_1(u) - F_1^{\text{PB}}(u)]. \end{aligned} \quad (3.38)$$

In the second line, we set $u = \ln(r/b)$ with $u_c = \ln(r_c/b)$ being the upper bound and define

$$\begin{aligned} F_1 &= 2\pi r^2 \ell_{B0} n_1, \\ F_1^{\text{PB}} &= 2\pi r^2 \ell_{B0} n_1^{\text{PB}}, \end{aligned} \quad (3.39)$$

as in Eq.(2.17). These quantities are treated as functions of u . In the bottom plates of Fig.7, we shall see that u_c may be pushed to infinity since the integrand in the second line of Eq.(3.38) vanishes for large u .

6. Criteria of strong deformations of the counterion distribution

We examine the conditions of strong attraction of the counterions due to a composition change around the rod. We assume that ϕ_B is not very small and ξ is not much separated from a for simplicity. If $g_1 \gg 1$, $\delta\phi$ is of order $g_1 a / 2\pi\ell_{Bb}$ at $r \sim \xi$ from Eq.(3.33). Since $n_1 \propto e^{g_1\phi}$ from Eq.(3.18), an appreciable attraction of the counterions is induced due to the composition change when

$$g_1^2 a / 2\pi\ell_{Bb} \gtrsim 1. \quad (3.40)$$

For large $g_1 \gg 1$ the above condition can be realized while $\delta\phi$ remains small ($\ll \phi_B$).

Also $\phi'(b)$ satisfies the boundary condition (3.27). This yields a contribution to $\delta\phi(r)$, written as $(\delta\phi)_b(r)$. It obeys $(1 - \xi^2 \nabla^2)(\delta\phi)_b = 0$ in the bulk, so it decays rapidly far from the rod. If $\xi \lesssim b$, it is approximately written as

$$(\delta\phi)_b(r) \cong \left[\gamma + \frac{\Delta_1 \sigma}{2\pi b} \right] \frac{\xi}{C} \exp \left[-\frac{r-b}{\xi} \right]. \quad (3.41)$$

If the above composition change is positive, the counterions are significantly attracted to the rod when

$$g_1 (\gamma + \Delta_1 \sigma / 2\pi b) \xi / C \gtrsim 1. \quad (3.42)$$

If it is negative and its absolute value exceeds unity and if the condition (3.40) does not hold, the counterions should be repelled from the rod.

The criterions (3.40) and (3.42) are crude ones based on many assumptions. In particular, $F_1(b) \sim 1$ has been assumed in deriving Eq.(3.40) and the unknown $\sigma = \sigma_0\alpha$ is contained in Eq.(3.42). Setting up general criterions is at present difficult, because many of the parameters strongly affect the counterion distribution. Nevertheless, we recognize that the counterion distribution can be changed dramatically even for a slight change of the composition in the strong solvation condition $|g_1| \gg 1$.

C. Numerical results in the Ginzburg-Landau theory for water-oil solvent without salt

We present some numerical results for a water-oil solvent without salt. In all the examples to follow, we numerically solve Eqs.(3.14), (3.17), (3.18), and (3.21) under given boundary conditions by setting

$$\begin{aligned} b &= 2a, \quad R/b = e^6 \cong 403, \\ \sigma_0 &= \pi/2a, \quad C = 3/a, \quad \Delta_1 = 7, \\ \varepsilon_1 &= 2\varepsilon_0, \quad \ell_{B0} = 12a/\pi = 6/\sigma_0, \end{aligned}$$

where ℓ_{B0} is defined in Eq.(3.32). The solvation parameter g_1 will be either of 5, 7, and 10, while it can be larger in real situations (see the discussion below Eq.(3.28)). The parameter $A = 2\pi\ell_{B0}b^2K_0$ in Eq.(2.28) will be chosen to be small. As a result, little ionization occurs without composition variations near the rod. In our simulation the counterion density far from the rod is so small such that its effect on the bulk solvent phase diagram is negligible²⁵.

1. Attraction of water and counterions to a hydrophobic rod

The interaction between the solvent and the rod in Eq.(3.10) leads to the boundary condition (3.27) in our gradient theory. For $\gamma < 0$ ($\gamma > 0$), the rod repels (attracts) the water component and is hydrophobic (hydrophilic) without ionization. Even for $\gamma < 0$, however, the right hand side of Eq.(3.27) changes from positive to negative with increasing the degree of ionization α and the condition (3.42) can eventually hold for $|\gamma| < \Delta_1\sigma/2\pi b$. Then the rod becomes effectively hydrophilic. To examine the resultant preferential adsorption of the water-like component, we introduce

$$\Gamma = 2\pi \int_b^R dr r [\phi(r) - \phi_B], \quad (3.43)$$

where ϕ_B is the value of $\phi(r)$ at $r = R$.

Figure 7 illustrates such a changeover in the one phase region comparing two cases, (a) $a^2\gamma = -0.6$ and (b) $a^2\gamma = -0.2$. We set $\chi = 1.4$, $\phi_B = 1/3$, $g_1 = 5$, and $v_0K_0 = 10^{-4}$. Then $A = 2\pi\ell_{B0}b^2K_0 = 0.0096$ from Eq.(2.28), $\xi = 1.32a$ from Eq.(3.30), and $v_0K = 10^{-4}e^{12\phi_s}$ from Eq.(3.20). The left hand side of Eq.(3.40)

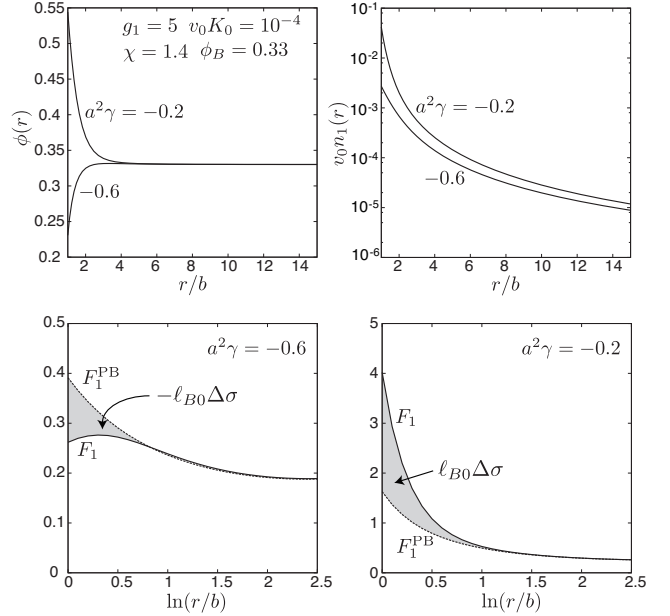


FIG. 7: Numerical results for a mixture solvent in the salt-free case for $\chi = 1.4$, $\phi_B = 1/3$, $g_1 = 5$, and $A = 0.0096$ (on the point (+) in Fig.9). Top plates: composition $\phi(r)$ (left) and normalized counterion density $v_0 n_1(r)$ (right) for $a^2\gamma = -0.6$ and -0.2 . Bottom plates: $F_1(u)$ and $F_1^{\text{PB}}(u)$ in Eq.(3.39) vs $u = \ln(r/b)$ for $a^2\gamma = -0.6$ (right) and -0.2 (left). The area between these two functions (shaded) is equal to the normalized excess charge density $\ell_{B0}\Delta\sigma$ from Eq.(3.38).

is 1.73, while the left hand side of Eq.(3.42) is -0.609 in (a) and 0.755 in (b). However, $F_1(b) = 0.109$ in (a) and 1.54 in (b), so the criterion (3.40) is not justified for (a) (see the discussion above Eq.(3.32)). In the upper left panel of Fig.7, we present the composition profile $\phi(r)$ near the rod, which is repelled in (a) and attracted in (b). However, as shown in Eq.(3.33), $\delta\phi = \phi - \phi_B$ has a positive tail (r^{-2}) without salt, giving rise to a positive logarithmic contribution $\sim (g_1 a \xi^2 / \ell_{B0}) \ln(R/\xi)$ to the integral Γ in Eq.(3.43). Due to this singular contribution we obtain $\Gamma = 0.706a^2$ in (a), while $\Gamma = 3.99a^2$ in (b). In the upper right panel, the difference of $n_1(r)$ between the two cases is large and $n_1(r)$ is written on a semi-logarithmic scale. Here, $\alpha = 0.369$, $\phi(b) - \phi_B = -0.101$, and $v_0 n_1(b) = 2.73 \times 10^{-3}$ in (a), while $\alpha = 0.621$, $\phi(b) - \phi_B = 0.214$, $v_0 n_1(b) = 4.19 \times 10^{-2}$ in (b). The lower panels of Fig.7 display the two functions $F_1(u)$ and $F_1^{\text{PB}}(u)$ in Eq.(3.39) for the two cases. The excess charge density in Eq.(3.38) is negative as $\Delta\sigma = -0.02/\ell_{Bb} = -0.03/\ell_{B0}$ in (a), but is positive as $\Delta\sigma = 0.33/\ell_{Bb} = 0.56/\ell_{B0}$ in (b).

2. First order phase transition of ionization without salt

In the right panel of Fig.8, we vary ϕ_B at fixed χ on the lines (A)-(E), where $g_1 = 10$, $a^2\gamma = -0.4$, and $v_0K_0 = 8 \times 10^{-6}$. We set $\chi = 2.2$ (A), 1.7 (B), 1.3

(C), 1.16 (D), and 1 (E). With varying ϕ_B , we find a first order phase transition of ionization for χ larger than a critical value χ^{cri} . That is, there are two branches of weak and strong ionization for $\chi > \chi^{\text{cri}}$ around the transition-point $\phi_B = \phi_B^{\text{tra}}(\chi)$ dependent on χ , while there is no discontinuity for $\chi \leq \chi^{\text{cri}}$. In the left panel of Fig.8, the grand potential Ω in Eq.(3.23) is lower on the equilibrium branch than on the metastable one. In the right panel of Fig.8, a first order phase transition line starts from a point given by $(\phi_B, \chi) = (0.1736, 2.390)$ on the bulk coexistence curve and ends at a critical point given by $(\phi_B, \chi) = (\phi_B^{\text{cri}}, \chi^{\text{cri}}) = (0.415, 1.16)$, where $\phi_B^{\text{cri}} = \phi_B^{\text{tra}}(\chi^{\text{cri}})$.

This first order phase transition occurs over a wide range of the parameters both with and without salt. In more expanded Fig.9, the first order phase transition lines are displayed for various g_1 and γ without salt, which start from a point on the bulk coexistence curve and end at an ionization critical point. These lines are markedly enlarged with increasing the hydrophilic solvation strength ($g_1 > 0$) and/or the rod hydrophobicity ($\gamma < 0$).

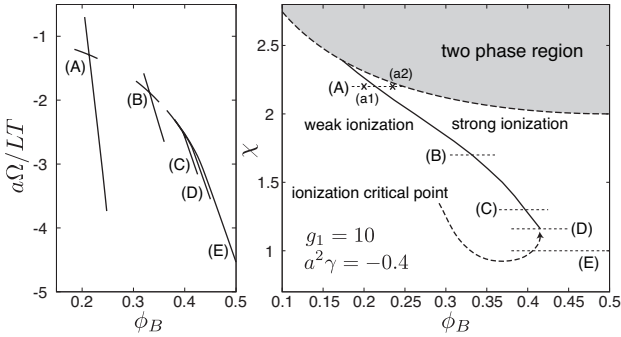


FIG. 8: Left; Normalized grand potential $a\Omega/LT$ on lines of constant χ , (A)-(E), where $g_1 = 10$, $K_0v_0 = 8 \times 10^{-6}$, and $a^2\gamma = -0.4$ for water-oil solvent without salt. For (A)-(C) there are two branches of weak and strong ionization and the equilibrium is given by the lower branch, while for (D) and (E) there is only one branch. Right: Resultant phase diagram in the ϕ_B - χ plane for this choice of the parameters, where a first order phase transition line ends at a critical point.

In Figs. 10-13, we examine the phase transition in detail. The parameter values are $g_1 = 10$, $a^2\gamma = -0.4$, and $v_0K_0 = 8 \times 10^{-6}$ as in Fig.8.

(i) In Fig. 10, the degree of ionization α vs ϕ_B is shown for the lines (A)-(E), where (A)-(C) pass through the first order phase transition line $\phi_B = \phi_B^{\text{tra}}(\chi)$, (D) passes through the critical point at $(\phi_B, \chi) = (\phi_B^{\text{cri}}, \chi^{\text{cri}})$, and (E) is a supercritical path.

(ii) The left panels of Fig.11 show the charge density σ and the effective charge density σ_{eff} multiplied by ℓ_{Bb} as functions of ϕ_B on the lines (A) and (C), where ℓ_{Bb} is defined in Eq.(3.32) and σ_{eff} by Eq.(3.37). At the transition from weak to strong ionization, $\ell_{Bb}\sigma$ increases but $\ell_{Bb}\sigma_{\text{eff}}$ decreases in these cases. Here the counterions are

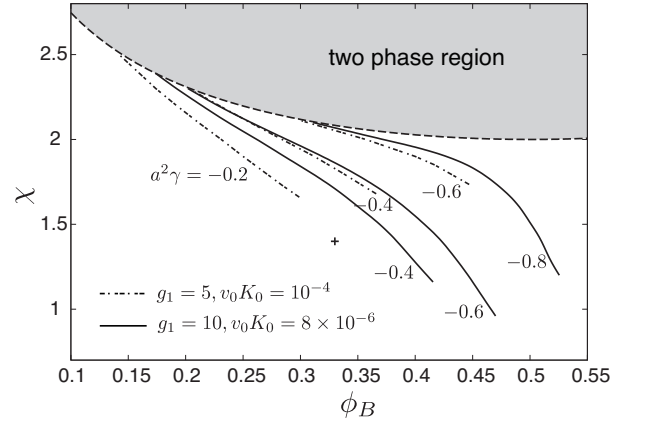


FIG. 9: First-order phase transition lines of ionization in the ϕ_B - χ plane for various parameter values without salt. Solid lines: $a^2\gamma = -0.4, -0.6$, and -0.8 with $g_1 = 7$ and $K_0v_0 = 8 \times 10^{-6}$. Broken lines: $a^2\gamma = -0.2, -0.4$, and -0.6 with $g_1 = 5$ and $K_0v_0 = 10^{-4}$. Each line starts from a point on the bulk coexistence curve and ends at a critical point with decreasing χ in the bulk one-phase region.

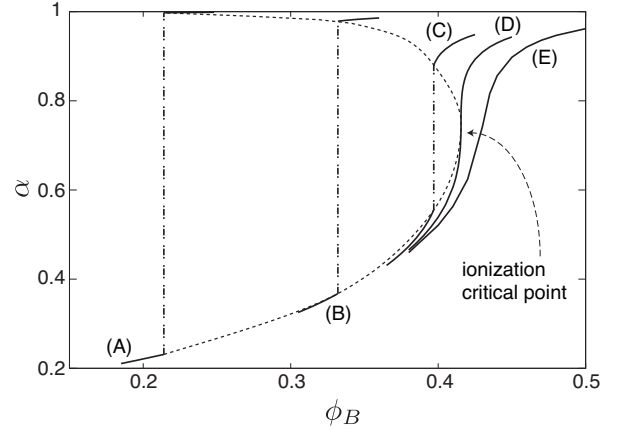


FIG. 10: Degree of ionization α vs ϕ_B without salt along the lines (A)~(E) in Fig.8, where $g_1 = 10$, $K_0v_0 = 8 \times 10^{-6}$, and $a^2\gamma = -0.4$. The discontinuity (broken line segments) vanishes at the critical point of ionization.

more strongly attracted to the rod in the strongly ionized phase than in the weakly ionized phase, as will be evident in Fig.12. The right panels of Fig.11 display the counterion density on the outer surface $n_1(R) = \Pi/T$ as a function of ϕ_B . It is counter-intuitive in these cases that Π decreases discontinuously at the transition with increasing α .

(iii) In Fig.12, space profiles of ϕ , n_1 , F_1 , and F_1^{PB} are given at the two points (a1) and (a2) in the two phases on the line (A) in Fig.8 in the same manner as in Fig.7. The right hand sides of Eqs.(3.40) and (3.42) are equal to 5.83 and -0.877 for (a1) and to 6.13 and 2.53 for (a2), respectively. Here, $\alpha = 0.221$, $\phi_b = 0.143$, $v_0n_1(b) = 3.20 \times 10^{-4}$, $\Delta\sigma = -0.003/\ell_{Bb} = -0.004/\ell_{B0}$,

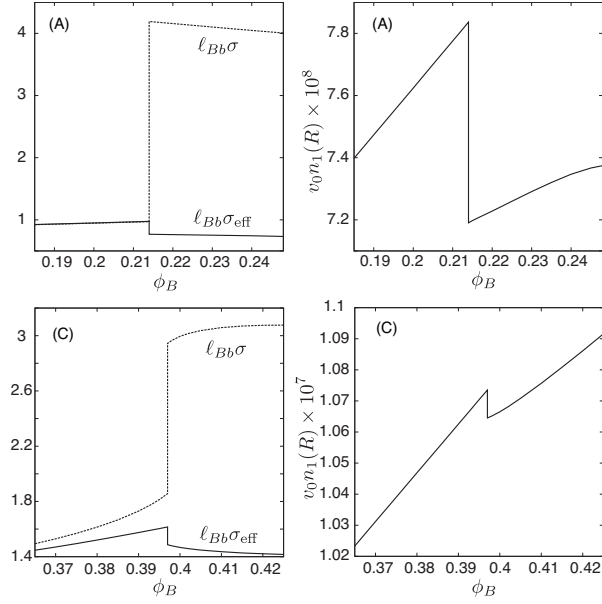


FIG. 11: Charge density σ and effective charge density σ_{eff} in Eq.(3.29) on the rod around the transition in units of ℓ_{Bb}^{-1} (left). Counterion density $n_1(R) = \Pi/T$ on the outer surface in units of v_0^{-1} (right). These are plotted as functions of ϕ_B on the line (A) (upper plates) and on the line (C) (lower plates) in Fig.8. In the weakly ionized phase, $\ell_{Bb}\sigma$ is smaller than unity for (A) and larger than unity for (C), leading to larger discontinuities for (A) than for (C).

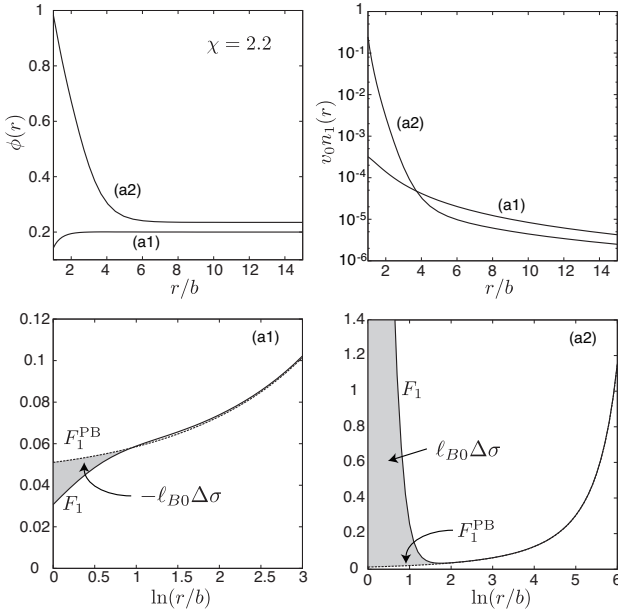


FIG. 12: Profiles without salt at the two points (a1) (weakly ionized state) and (a2) (strongly ionized state) on the line (A) in Fig.8. Top plates: $\phi(r)$ (left) and $v_0 n_1(r)$ (right) vs r/b . Bottom plates: F_1 and F_1^{PB} vs $\ln(r/b)$ for (a1)(left) and (a2)(right). From Eq.(3.38) the area of the gray region is equal to $-\ell_{B0}\Delta\sigma$ for (a1) and to $\ell_{B0}\Delta\sigma$ for (a2).

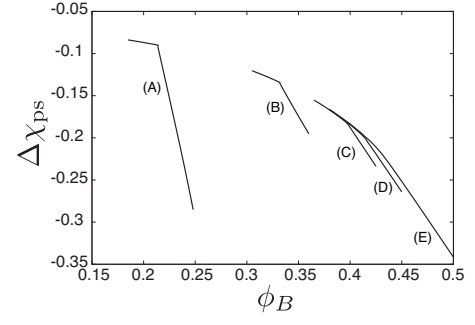


FIG. 13: Change of the effective polymer-solvent interaction parameter $\Delta\chi_{ps}$ due to ionization for a two component solvent without salt along the paths (A)-(E) in Fig.8.

and $\Gamma = 0.706a^2$ at (a1), while $\alpha = 0.998$, $\phi_b = 0.982$, $v_0 n_1(b) = 0.245$, $\Delta\sigma = 3.32/\ell_{Bb} = 4.89/\ell_{B0}$, and $\Gamma = 3.99a^2$ at (a2). The upper left panel shows that the water component is considerably depleted from the rod at (a1) but it covers the rod almost completely at (a2). The upper right panel indicates that the counterions are more accumulated around the rod at (a2) than at (a1) such that they are more depleted far from the rod at (a2) than at (a1).

(iv) In Fig.13, we plot the change of the effective polymer-solvent interaction parameter $\Delta\chi_{ps}$ along the paths (A)-(E). It is defined by Eq.(2.37), where Ω is given by Eq.(3.23). The second term $\pi R^2 n(R)$ in the brackets of Eq.(2.37) is at most 10% of the first term Ω/TL and its discontinuity at the transition is so small and is not clearly seen in the figure.

Note that the grand potential Ω in Eq.(3.23) consists of three characteristic parts. Namely, in the right hand side of Eq.(3.23), the first line represents the composition part, the first two terms in the second line the dissociation part, and the third term the electrostatic part. At the ionization transition from a weakly to strongly ionized state, the composition part increases due to the layer formation, while the dissociation part decreases. Compared to these two changes, the change of the electrostatic part is much smaller in our analysis. In fact, at the transition point on the line A, these three parts (multiplied by a) are given by $(0.848, -0.775, -1.36)$ and $(11.0, -11.0, -1.28)$ in the weakly and strongly ionized states, respectively. At the transition point on the line C, the corresponding three parts are given by $(2.56, -2.14, -2.93)$ and $(5.17, -4.72, -2.96)$.

3. Profiles near the bulk coexistence curve without salt

In Figs.8 and 9, the line of the first order ionization phase transition starts from the coexistence curve. In the prewetting phase transition on a planar wall^{30,31,32}, a first order phase transition line also starts at the coexistence curve, where the adsorption is weak in the weakly

adsorbed phase even on the coexistence curve but it is logarithmically divergent on approaching the coexistence curve in the strongly adsorbed phase.

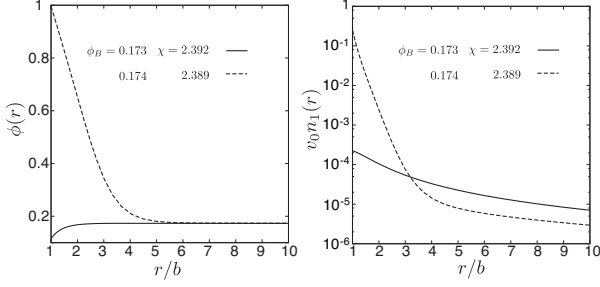


FIG. 14: Composition $\phi(r)$ and normalized counterion density $v_0 n_1(r)$ on the coexistence curve for $(\phi_B, \chi) = (0.1730, 2.392)$ in the weakly ionized phase (bold lines) and $(0.1740, 2.389)$ in the strongly ionized phase (dotted lines). The line of the first order ionization phase transition starts between these two points as in the right panel of Fig.8.

In the following we examine the profiles of $\phi(r)$ and $n_1(r)$ close to the water-poor branch of the coexistence curve ($\phi_B \leq 1/2$). We vary ϕ_B and χ fixing the other parameters as in Figs.8 and 10-13. Namely, $g_1 = 10$, $a^2\gamma = -0.4$, and $v_0 K_0 = 8 \times 10^{-6}$.

(i) Figure 14 presents the profiles at two points, $(\phi_B, \chi) = (0.1730, 2.392)$ and $(0.1740, 2.389)$ on the coexistence curve between the transition point $(\phi_B, \chi) = (0.1736, 2.390)$. We recognize marked jumps at the transition. That is, at the weakly ionized state at $\phi_B = 0.173$, we have $\alpha = 0.202$, $\sigma = 1.21\ell_{B0}^{-1} = 0.900\ell_{Bb}^{-1}$, and $\Gamma = 0.565a^2$, while at the strongly ionized state at $\phi_B = 0.174$, we have $\alpha = 0.999$, $\sigma = 5.99\ell_{B0}^{-1} = 4.44\ell_{Bb}^{-1}$, and $\Gamma = 27.2a^2$. The first component remains repelled around the rod in the weakly ionized phase but is much attracted around it in the strongly ionized phase.

(ii) In the top panels of Fig.15, we set $\phi_B = 0.4$ to obtain $\Gamma/a^2 = 28.9, 65.2$, and 156 for $\chi = 1.9, 2.0$, and 2.027 , respectively. In the middle panels, we set $\phi_B = 0.45$ to obtain $\Gamma/a^2 = 86.6, 178$, and 497 for $\chi = 1.9, 2.0$, and 2.0067 , respectively. The points $(\phi_B, \chi) = (0.4, 2.027)$ and $(0.45, 2.0067)$ are on the coexistence curve. In the bottom plate, we set $\phi_B = 0.5$ to obtain $\Gamma/a^2 = 88.9, 211.0$, and 8691 for $\chi = 1.97, 1.990$, and 2.0 , respectively. At the critical point $\phi_B = 0.5$ and $\chi = 2$, the excess deviation $\delta\phi(r) = \phi(r) - \phi_B$ decays as $\delta\phi(r) \sim r^{-1}$ for $r/a \lesssim 10$ and $\delta\phi(r) \sim r^{-2}$ for $10 \lesssim r/a \lesssim 50$ (left). In all these cases, the dissociation is nearly complete or $\alpha \cong 1$.

Furthermore, for $(\phi_B, \chi) = (0.45, 2.03)$, we can see a shoulder in $\phi(r)$ in Fig.15 (left in the middle). It represents a water-rich layer varying gradually with no sharp interface. In a more drastic manner, Marcus *et al.*⁴³ recently obtained a water-rich layer separated from the water-poor bulk region by a sharp boundary around a rod or a sphere. They assumed the homogeneity of $h = f'_0(\phi) - \varepsilon_1 E^2/8\pi$ only, where the gradient term

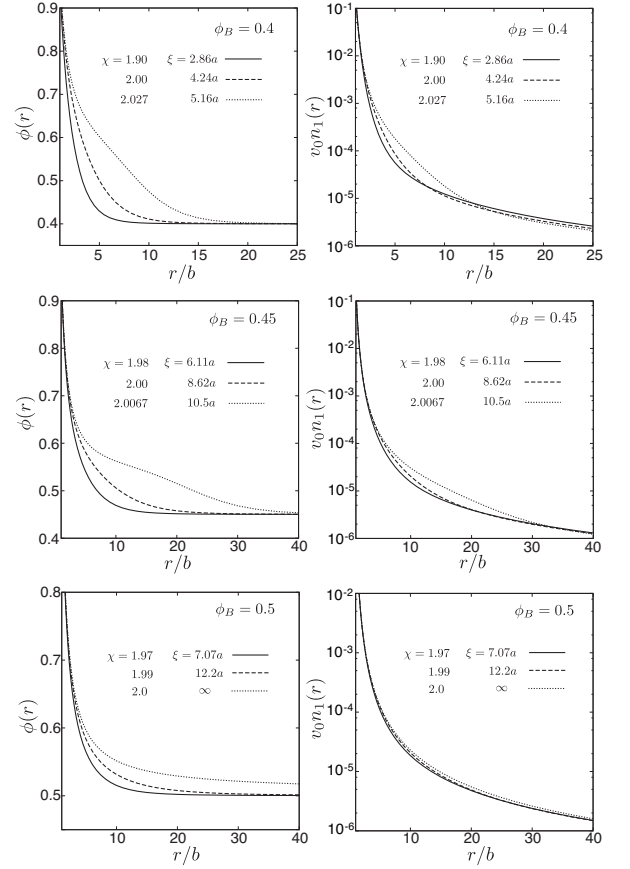


FIG. 15: Composition $\phi(r)$ and normalized counterion density $v_0 n_1(r)$ near the bulk coexistence curve for $\phi_B = 0.4$ (top), 0.45 (middle), and 0.5 (bottom). Values of χ and ξ are given within each panel.

and the free ions were both neglected (compare it with Eq.(3.21)). Also in our scheme, such a sharp layer with an interface is produced in the low density limit of the counterions (realized for very large R) and under the conditions $\gamma = \Delta_1 = 0$ (which yields the boundary condition $\phi(b) = 0$ from Eq.(3.27)).

In addition, if the bulk region is in a metastable state (inside the bulk coexistence curve), a solvation layer around a polymer chain can trigger macroscopic phase separation. This is analogous to the nucleation process around a charge particle in polar fluids⁴⁴.

IV. SUMMARY AND REMARKS

In this paper, the ion distributions have been examined when the degree of ionization $\alpha = \sigma/\sigma_0$ is a fluctuating variable. Here σ and σ_0 are the line density of ionized monomers and that of ionizable monomers, respectively. In mixture solvents, the counterion and composition profiles have turned out to be extremely complex, sensitively depending on the interaction parameters and the average

composition, owing to the preferential solvation.

In Section II, a long ionizable rod in a one-component solvent has been treated without and with salt, where the dissociation process gives rise to the free energy contribution F_d in Eq.(2.8). Minimization of the grand potential Ω in Eq.(2.9) has then yielded α obeying the mass action law and the charge distribution $n_1(r)$ obeying the Poisson-Boltzmann equation. In Subsection IIB, we have examined the counterion density at the rod surface without salt on the basis of the previous exact results in the literature³⁵. For considerably large $M = \ln(R/b)$, α is determined by Eq.(2.30) for $(1 - \sigma\ell_B)M \gg 1$ and by Eq.(2.31) for $(\sigma\ell_B - 1)M \gg 1$. All the quantities sensitively depend on the parameter $A(\propto K_0)$ in Eq.(2.28) as in Fig.3. In the limit $M \gg 1$, α tends to unity in the former and to a well-defined limit in the range $(\ell_B\sigma_0)^{-1} < \alpha < 1$ in the latter as in Fig.4. In Subsection IIC, we have added a salt, where the cations are of the same species as the counterions from the rod. The ion distribution is homogeneous far from the rod as in Fig.5, while α decreases to zero with increasing the salt concentration as in Fig.6.

In Section III, a charged rod in two component solvents has been treated without salt. In Subsection IIIA, we have presented a simple theory of the solvation shell formation at very small concentration of a water-like solute in a less polar solvent. Addition of a small amount of the water-like component can much enhance ionization. In Subsection IIIB, we have then generalized our theory in Section II to describe the ionization equilibrium in two component solvents. The additional free energy contribution is ΔF in Eq.(3.10) for the composition ϕ , which includes the solvation couplings with ions ($\propto g_i$) and the ionized monomers ($\propto \Delta_1$). Though still fragmentary, Subsection IIIC has presented numerical results without salt, where the solvent consists of a water-like component and a less polar component. The counterions and the charged monomers are hydrophilic with $g_1 > 0$ and $\Delta_1 > 0$. In Fig.7, even if a rod is hydrophobic without ionization ($\gamma < 0$), it becomes effectively hydrophilic with ionization. In Figs.8-12, we have found a first order phase transition of ionization for hydrophilic counterions around a hydrophobic rod. In Fig.13, the polymer-solvent interaction parameter χ_{ps} decreases upon ionization. Finally, we have examined the composition and counterion profiles at the crosspoint of the ionization transition line and the coexistence curve in Fig.14 and near the coexistence curve in the strongly ionized phase in Fig.15. The preferential adsorption Γ in Eq.(3.43) much increases near the coexistence curve in the strongly ionized phase.

In our theory, two parameters have been introduced, which characterize polyelectrolytes. First, we have defined the change of the effective polymer-solvent interaction parameter $\Delta\chi_{ps}$ due to dissociation in Eq.(2.37). Its behavior has been examined analytically in the one-component case and numerically in Fig.13 in the two-component case. Its negativity indicates increases of the

solubility and the gyration radius with ionization. Second, we have derived the mass action law around polymer backbones in Eq.(2.15) for one component solvents and in Eq.(3.19) for mixture solvents. It is characterized by the dissociation constant K , which depends on various parameters. However, we do not know such data for polyelectrolytes, while the dissociation constant has been measured for chemical reactions taking place in the bulk region of fluid mixtures^{39,40}.

We make further remarks. Some of them are related to previous and proposed experiments.

- (i) The first order phase transition of ionization is expected particularly for polymers which are hydrophobic without ionization and hydrophilic with ionization. Upon a transition from weakly to strongly ionized states, the number of the counterions increase, but the osmotic pressure has decreased in our examples in Fig.11. A polymer chain can be in an expanded coil state in a weakly ionized state and be in a more expanded state after the transition. On the other hand, if a polymer chain is in a shrunken globule state in a weakly ionized state, a coil-globule transition might take place simultaneously with the ionization transition.
- (ii) Though not shown in this work, the first order phase transition of ionization occurs even with a small amount of salt. However, we do not know the effects of adding salt in mixture solvents in detail.
- (iii) We have also found a similar first order transition on a planar boundary wall with ionizable groups. We should investigate the effects of dissociation and/or salt on the prewetting transition on a solid plate^{30,31,32}. Its theory will be reported shortly.
- (iv) We are interested in the conformation of an ionizable polymer chain near the consolute critical point of a polar binary mixture. A number of papers have been devoted to study the conformation of a neutral polymer chain near the solvent critical point^{45,46,47}. The effect of the composition fluctuations is much enhanced on a charged polymer chain due to the preferential solvation.
- (v) In a mixture of water+isobutylic acid (IA), Bonn *et al.*⁴⁰ observed a dramatic decrease of the conductivity with increasing the IA content. In this system IA partly dissociates into H^+ and Butyrate $^-$ ions and their finding suggests formation of an ion-induced mesophase. In near-critical binary mixtures with salt, many experimental groups have observed mesoscopic ion-induced aggregates⁴⁸. In polyelectrolytes, similar heterogeneities have been observed for a long time^{49,50,51}. In these phenomena, relevance is the preferential solvation.
- (vi) In polyelectrolytes, we may replace counterions by hydrophobic ions^{36,42} such as tetraphenylarsonium Ph_4As^+ , tetrabutylammonium TBA^+ , or tetrarphenylborate BPh_4^- . Hydrophobic ions will be repelled from the polymer backbone if water is enriched in its vicinity. For hydrophilic and hydrophobic ion pairs, the influence of the preferential solvation can be much more enhanced than for hydrophilic ion pairs²⁶. In fact, in a mixture of $D_2O + 3$ -methylpyridine, Sadakane *et al.*⁵²

recently added sodium tetrphenylborate NaBPh_4 to find mesophases by small-angle-neutron scattering.

Acknowledgments

This work was supported by Grants-in-Aid for scientific research on Priority Area “Soft Matter Physics” and the Global COE program “The Next Generation of Physics, Spun from Universality and Emergence” of Kyoto University from the Ministry of Education, Culture, Sports, Science and Technology of Japan. The authors thank K. Yoshikawa, T. Sumi, Y. Masubuchi, and Y. Yamasaki for valuable discussions.

Appendix: Calculation in the one-component solvent case without salt

We first calculate Ω in Eq.(2.14). Equation (2.17) gives the electric field

$$E = -\frac{T}{e} \frac{dU}{dr} = \frac{T}{e} \left[\frac{d}{dr} \ln F_1 - \frac{2}{r} \right]. \quad (\text{A1})$$

We express the electrostatic energy $F_e = \int dr \varepsilon E^2 / 8\pi$ as

$$F_e = TL\sigma + TL\ell_B^{-1} \mathcal{F}_e(\ell_B\sigma), \quad (\text{A2})$$

where the scaling function $\mathcal{F}_e(s)$ with $s = \ell_B\sigma$ appears in Eq.(2.26). For $\sigma < \sigma^*$ the first lines of Eqs.(2.20) and (2.21) yield

$$\mathcal{F}_e(s) = (1 + B^2)M + \ln \left[1 + \frac{s^2 - 2s}{1 - B^2} \right]. \quad (\text{A3})$$

For $\sigma > \sigma^*$ the second lines of Eqs.(2.20) and (2.21) yield

$$\mathcal{F}_e(s) = (1 - B^2)M + \ln \left[1 + \frac{s^2 - 2s}{1 + B^2} \right]. \quad (\text{A4})$$

Here B depends on $M = \ln(R/b)$ and $s = \ell_B\sigma$ as in Eq.(2.21). For $|q| \gg 1$ we obtain the approximate expressions in eq.(2.27). At $\sigma = \sigma^*$ we have $s = M/(1+M)$ and $\mathcal{F}_e = M - 2 \ln(1+M)$.

* Electronic address: okamoto'r@sphys.kyoto-u.ac.jp

† Electronic address: onuki@sphys.kyoto-u.ac.jp

¹ G.S. Manning, J. Chem. Phys. **51**, 924 (1969); J. Phys. Chem. B **111**, 8554 (2007).

² F. Oosawa, Polyelectrolytes (Marcel Dekker, New York, 1971).

³ J.L. Barrat and J.F. Joanny, Adv. Chem. Phys. XCIV, I. Prigogine, S.A. Rice Eds., John Wiley & Sons, New York 1996.

⁴ Y. Levin, Rep. Prog. Phys. **65**, (2002) 1577.

⁵ N. Volk, D. Vollmer, M. Schmidt, W. Oppermann, and K. Huber, Adv. Polym. Sci. **166**, 29 (2004).

⁶ C. Holm, J. F. Joanny, K. Kremer, R. R. Netz, P. Reineker, C. Seidel, T. A. Vilgis, and R. G. Winkler, Adv. Polym. Sci. **166**, 67 (2004).

⁷ A.V. Dobrynin and M. Rubinstein, Prog. Polym. Sci. **30**, 1049 (2005).

⁸ W. Essafi, F. Lafuma, D. Baigl, and C. E. Williams, Europhys. Lett. **71**, 938 (2005).

⁹ D. Andelman, Proceeding of the Nato ASI and SUSSP on "soft condensed matter in molecular and cell biology", (2005), ed. by W. Poon and D. Andelman, (Taylor & Francis, New York, 2006), pp. 97-122.

¹⁰ A. Naji and R. Netz, Phys. Rev. E **73**, 056105 (2006).

¹¹ E. Raphael and J. F. Joanny, Europhys. Lett. **13**, 623 (1990).

¹² I. Borukhov, D. Andelman, and H. Orland, Europhys. Lett. **32**, 499 (1995).

¹³ I. Borukhov, D. Andelman, R. Borrega, M. Cloitre, L. Leibler, and H. Orland, J. Phys. Chem. B **104**, 11027 (2000).

¹⁴ M. Muthukumar, J. Chem. Phys. **120**, 9343 (2004).

¹⁵ A. Onuki and R. Okamoto, J. Phys. Chem. B, **113**, 3988 (2009).

¹⁶ C. B. Post and B. H. Zimm, Biopolymers **21**, 2139 (1982).

¹⁷ P. G. Arscott, C. Ma, J. R. Wenner and V. A. Bloomfield, Biopolymers, **36**, 345 (1995).

¹⁸ A. Hultgren and D. C. Rau, Biochemistry **43**, 8272 (2004).

¹⁹ C. Stanley and D. C. Rauy, Biophys. J. **91**, 912 (2006).

²⁰ S. Flock, R. Labarbe, and C. Houssier, Biophysical Journal **70**, 1456 (1996).

²¹ D. Baigl and K. Yoshikawa, J. Biophys. **88**, 3486 (2005).

²² D. Ben-Yaakov, D. Andelman, D. Harries, and R. Podgornik, J. Phys. Chem. B **113** 6001 (2009).

²³ J. N. Israelachvili, *Intermolecular and Surface Forces* (Academic Press, London, 1991).

²⁴ A. Onuki and H. Kitamura, J. Chem. Phys. **121**, 3143 (2004).

²⁵ A. Onuki, Phys. Rev. E **73**, 021506 (2006).

²⁶ A. Onuki, J. Chem. Phys. **128**, 224704 (2008).

²⁷ Y. Tsori and L. Leibler, Proc. Natl. Acad. Sci. U.S.A. **104**, 7348 (2007)

²⁸ M. Bier, J. Zwanikken, and R. van Roij, Phys. Rev. Lett. **101**, 046104 (2008); J. Zwanikken, J. de Graaf, M. Bier, and R. van Roij, J. Phys.: Condens. Matter **20**, 494238 (2008).

²⁹ A. Onuki, Europhys. Lett. **82**, 58002 (2008).

³⁰ J. W. Cahn, J. Chem. Phys. **66** 3667 (1977).

³¹ C. Ebner and W. F. Saam, Phys. Rev. Lett. **38**, 1486 (1977).

³² P. Tarazona and R. Evans, Mol. Phys. **48**, 799 (1983).

³³ A. Onuki, *Phase Transition Dynamics* (Cambridge University Press, Cambridge, 2002)

³⁴ For ideal gases the entropic free energy is of the form $Tn_i[\ln(n_i v_{0i}) - 1]$ with $v_{0i} = \hbar^3(2\pi/m_i T)^{3/2}$, where \hbar is the Planck constant and m_i is the particle mass. This term is larger than that in Eq.(2.7) by $n_i \Delta\mu_i$, where $\Delta\mu_i = T \ln(v_{0i}/v_0)$ is a constant shift of the chemical potential of the i th ions.

³⁵ R. M. Fuoss, A. Katchalsky, and S. Lifson, Proc. Natl.

- Acad. Sci. U.S.A., **37**, 579 (1951).
- ³⁶ T. Osakai and K. Ebina, *J. Phys. Chem. B* **102**, 5691 (1998).
- ³⁷ A. Hamnett, C. H. Hamann, and W. Vielstich, *Electrochemistry* (Vch Verlagsgesellschaft Mbh, 1998).
- ³⁸ P. Debye and K. Kleboth, *J. Chem. Phys.* **42**, 3155 (1965).
- ³⁹ H. Ohtaki, *Bulletin of the Chemical Society of Japan*, **42**, 1573 (1969).
- ⁴⁰ D. Bonn, D. Ross, S. Hachem, S. Gridel, and J. Meunier, *Europhys. Lett.* **58**, 74 (2002).
- ⁴¹ M. Born, *Z. Phys.* **1**, 45 (1920).
- ⁴² Le Quoc Hung, *J. Electroanal. Chem.* **115**, 159 (1980).
- ⁴³ G. Marcus, S. Samin, and Y. Tsori, *J. Chem. Phys.* **129**, 061101 (2008).
- ⁴⁴ H. Kitamura and A. Onuki, *J. Chem. Phys.* **123**, 124513 (2005).
- ⁴⁵ P.G. de Gennes, *J. Phys. (Paris)* **37**, 59 (1976). Polymers can interact with two solvent components asymmetrically. There arises a pairwise attractive interaction among the monomers mediated by the critical fluctuations. Similar attractive interactions were derived among ions in mixture solvents by one of the present authors²⁵.
- ⁴⁶ A. Dondos and Y. Izumi, *Makromol. Chem.* **181**, 701 (1980).
- ⁴⁷ T. Sumi, K. Kobayashi, and H. Sekino, *J. Chem. Phys.* **127**, 164904 (2007).
- ⁴⁸ A. F. Kostko, M. A. Anisimov, and J. V. Sengers, *Phys. Rev. E* **70**, 026118 (2004).
- ⁴⁹ H. Matsuoka, D. Schwahn, and N. Ise, *Macromolecules* **24**, 4227 (1991).
- ⁵⁰ J. J. Tanahatoc and M. E. Kuil, *J. Phys. Chem. B* **101**, 5905 (1997).
- ⁵¹ B. D. Ermi and E. J. Amis, *Macromolecules* **31**, 7378 (1998).
- ⁵² K. Sadakane, H. Seto, H. Endo, and M. Shibayama, *J. Phys. Soc. Jpn.*, **76**, 113602 (2007); K. Sadakane, A. Onuki, K. Nishida, S. Koizumi, and H. Seto, preprint(arXiv:0903.2303v2).